Modeling of bias-field-dependent dielectric properties in ferroelectric thin films

C. K. Wong[a] and C. H. Tsang
Department of Applied Physics, The Hong Kong Polytechnic University, Hong Kong, China

F. G. Shin
Department of Applied Physics, Materials Research Center and Center for Smart Materials, The Hong Kong Polytechnic University, Hong Kong, China

(Received 16 February 2005; accepted 16 August 2005; published online 4 October 2005)

The bias-field-dependent dielectricity of ferroelectric thin films is studied by use of a multilayer model capable of modeling saturated and unsaturated hysteresis behavior under arbitrary fields. The simulated minor hysteresis loops at different bias fields are used to calculate the variation of dielectric permittivity with the bias field. The ε-E loops show asymmetric shifting along the field axis when the film is assumed to possess a secondary dielectric layer with trapped charge. Simulated D-E and ε-E loops are compared with the experimental data on barium zirconate titanate and lead zirconate titanate thin films. In general, the model predictions show reasonably good agreement with experiment. Effects of charge density and the ac measurement field amplitude on the measured permittivity, as well as the dielectric tunability have also been examined. © *2005 American Institute of Physics*. [DOI: 10.1063/1.2060950]

I. INTRODUCTION

In recent years, experimental studies of the bias-field-dependent dielectric properties in ferroelectric films have attracted great research interest because their tunable dielectric characteristics allow the development of capacitive devices.[1–4] Ferroelectrics possessing high tunability of permittivity can be used readily for tunable device applications. Moreover, reduction of device size is always desired for high-density usage and easy integration with other devices. With the advancements in fabrication and integration technology, research and development (R&D) in thin ferroelectric films is becoming quite intensified. Theoretical studies of the bias-field-dependent permittivity have also attracted great research interest in the literature. In modeling such properties, one notes that in reality the ferroelectric traces minor hysteresis loops under a small ac field, which is superimposed on a dc bias electric field. Therefore, an elaborate ferroelectric hysteresis model capable of modeling saturated and unsaturated loops in arbitrary fields is an essential tool to such a study. The model of Miller *et al.*,[5] adopted in our previous works to study ferroelectric films and composites,[6–8] can in principle simulate unsaturated hysteresis loops. This model is computationally efficient and most of the general features of hysteresis behavior in ferroelectrics can be reproduced. However, minor loops calculated from this model show strong aftereffect phenomenon when the applied field is not symmetric.[9] In other words, minor loops drift with time until steady state is reached. The drift magnitude can be quite large and is considered unphysical.[10] On the other hand, hysteresis models based on the Preisach model can faithfully model physical minor loops for arbitrary fields.[9,11] Therefore, a Preisach-type model is adopted in this work to study dielectric tunability in ferroelectric films.

On the other hand, measurement of hysteresis loops driven by a symmetric field may show anomalous horizontal offset for thin ferroelectric films. It has been widely accepted that this offset phenomenon is most likely not an intrinsic behavior of ferroelectric hysteresis loops. Possible origins have been suggested, such as oxygen vacancies,[12–15] lattice mismatch,[16] dopant, and illumination,[17] although it may very well be due to trapped charge carriers in the sample.[12,18–21] Similar horizontal shift phenomenon has also been observed in the measurement of bias-field-dependent dielectricity.[2,3] This is probably due to the same mechanisms as that observed in conventional hysteresis measurement.

In this article, theoretical simulations of hysteresis loops as well as the bias-field-dependent permittivity of thin ferroelectric films are performed with different applied field schedules. Following the techniques widely accepted in the literature, a thin ferroelectric film is assumed to possess a dead layer region (i.e., a weak ferroelectric/dielectric layer) which is presently modeled by a multilayer structure.[5,12,22] The simulated D-E loops are Fourier analyzed to obtain the bias-field dependence of dielectric permittivity. Numerical simulation of the permittivity is compared with the experimental data for lead zirconate titanate [$Pb(Zr_{0.52}Ti_{0.48})O_3$] (Ref. 1) and barium zirconate titanate [$Ba(Ti_{0.85}Zr_{0.15})O_3$] thin films.[2] The results will be shown to agree fairly well with the experimental data. In addition, the effects of charge density and the applied ac field amplitude on the simulated ε-E loops will also be examined.

II. MULTILAYER MODEL FOR THIN FERROELECTRIC FILMS

To study the dielectricity of a ferroelectric film, we will first model the hysteresis loops of the film. We assume a small nonferroelectric region (or dead layer) is formed at the ferroelectric film sample-electrode interface.[5,12,22] We also

[a]Electronic mail: wongck.ap@polyu.edu.hk

assume this nonferroelectric region can have trapped charge,[12,18–21] which is not necessarily uniform across the dead layer of the sample. In this work, we adopt a multilayered structure to model this configuration for thin films. The first layer in the multilayer model represents the bulk region of the film and the remaining m layers are for the dead layer region. This configuration allows us to conveniently model the trapped charge in the dead layer as the interfacial charge in between layers. The constitutive equations for the bulk and dead regions are

$$\begin{cases} D_f = \varepsilon_f E_f + P_f \\ D_{d,i} = \varepsilon_d E_{d,i}, \end{cases} \tag{1}$$

where D is electric displacement, ε is permittivity, E is electric field and P is polarization. Subscripts f and d denote the bulk region and the dead layer of the sample, respectively. i can be from 1 to m. In the literature, many investigators take $\varepsilon_d < \varepsilon_f$. We shall also apply this condition in the present study.

When an external electric field E_a is applied in the thickness direction across the film,

$$E_a = (1-\nu)E_f + \frac{\nu}{m}\sum_{j=1}^{m} E_{d,j}, \tag{2}$$

where ν represents the thickness ratio of the dead layer region in the ferroelectric thin film. As shown in Eq. (2), we assume for convenience that all constituent layers of the dead layer have even thicknesses. The boundary conditions for continuity of current density require

$$J = \sigma_f E_f + \partial D_f/\partial t = \sigma_d E_{d,i} + \partial D_{d,i}/\partial t, \tag{3}$$

where σ is electrical conductivity. Using Eqs. (1)–(3) and the relation $\partial P_f/\partial t = (\partial P_f/\partial E_f)(\partial E_f/\partial t)$, we obtain, after some manipulation,

$$\begin{aligned} (1-\nu)\left(\varepsilon_d \frac{\partial E_{d,i}}{\partial t} + \sigma_d E_{d,i}\right) &= \sigma_f E_a + \left(\frac{\partial P_f}{\partial E_f} + \varepsilon_f\right)\frac{\partial E_a}{\partial t} - \frac{\nu}{m}\sum_{j=1}^{m}\left[\sigma_f E_{d,j} \right. \\ &\left. + \left(\frac{\partial P_f}{\partial E_f} + \varepsilon_f\right)\frac{\partial E_{d,j}}{\partial t}\right]. \end{aligned} \tag{4}$$

Equation (4) constitutes m first-order differential equations. For a given external electric field E_a, we may obtain $E_{d,i}$ as a function of time t when the P-E relations for the bulk region is known, and E_f is calculated via Eq. (2). Then the measured electric displacement of the sample at a certain time t_0 can be obtained from current integration: $D(t_0) = \int_0^{t_0} J dt$.

Concerning the trapped charge in the dead layer, we use

$$\begin{cases} \rho_1 = D_{d,1} - D_f \\ \rho_{k+1} = D_{d,k+1} - D_{d,k}, \end{cases} \tag{5}$$

where ρ is the interfacial charge density and k can be from 1 to $m-1$. For experimental D-E or ε-E loops exhibiting horizontal shift, we assume the dead layer has trapped a finite amount of charge so that there is an internal electric-field buildup, thus the initial value for E_f and E_d can be calculated by Eqs. (1), (2), and (5) with E_a initially zero.

In this work, we have adopted a hysteresis model which is derived from the Preisach model.[11] The branch of the major (or saturated) hysteresis loop for increasing E_f is (see Appendix)

$$P^{+}_{f,\mathrm{sat}}(E_f) = \sum_{j=1}^{n} w_j P^{+}_{\mathrm{sat},j}(r_j, \upsilon_j), \tag{6}$$

where

$$\begin{aligned} P^{+}_{\mathrm{sat},j}(r_j,\upsilon_j) = \frac{P_s(1-r_j)\kappa}{8}\Bigg\{ & 2\coth\left(\frac{2h}{\upsilon_j}\right)\left[4\,\mathrm{csch}^2\left(\frac{2h}{\upsilon_j}\right)\ln\left(\frac{\cosh[(E_f-h)/\upsilon_j]}{\cosh[(E_f+h)/\upsilon_j]}\right) + \mathrm{sech}^2\left(\frac{E_f-h}{\upsilon_j}\right)\right] \\ & + 4\coth^3\left(\frac{2h}{\upsilon_j}\right)\tanh\left(\frac{E_f-h}{\upsilon_j}\right) + \mathrm{csch}^2\left(\frac{2h}{\upsilon_j}\right)\left[2\left(1+2\cosh\left(\frac{4h}{\upsilon_j}\right)\right)\mathrm{csch}^2\left(\frac{2h}{\upsilon_j}\right)\right. \\ & \times \ln\left(\frac{\cosh[(E_f-h)/\upsilon_j]}{\cosh[(E_f+h)/\upsilon_j]}\right) + \cosh\left(\frac{4h}{\upsilon_j}\right)\mathrm{sech}^2\left(\frac{E_f-h}{\upsilon_j}\right) + 2\left(\mathrm{sech}\left(\frac{2h}{\upsilon_j}\right) + \mathrm{csch}\left(\frac{2h}{\upsilon_j}\right)\right) \\ & \left. \times \mathrm{sech}\left(\frac{E_f+h}{\upsilon_j}\right)\sinh\left(\frac{E_f-h}{\upsilon_j}\right) + 2\left(2+\cosh\left(\frac{4h}{\upsilon_j}\right)\right)\tanh\left(\frac{E_f-h}{\upsilon_j}\right)\right]\Bigg\} + r_j P_{\mathrm{rev},j}(\upsilon_j), \end{aligned} \tag{7}$$

$$\kappa = \frac{-8\exp(-4h/\upsilon_j)\upsilon_j \sinh^4(2h/\upsilon_j)}{8h - 2\upsilon_j + 2(2h+\upsilon_j)\cosh(4h/\upsilon_j) - (4h+3\upsilon_j)\sinh(4h/\upsilon_j)}, \tag{8}$$

$$h = \upsilon_j \ln\sqrt{1 - 2\cosh^2(E_c/\upsilon_j) + 10\cosh(E_c/\upsilon_j)\sqrt{\cosh^2(E_c/\upsilon_j) - 1}}, \tag{9}$$

$$P_{\mathrm{rev},j}(v_j) = P_s \tanh(E_f/v_j), \tag{10}$$

and symbols P_s and E_c denote saturation polarization and coercive field, respectively. The descending major curve is taken as $P^-_{f,\mathrm{sat}}(E_f) = -P^+_{f,\mathrm{sat}}(-E_f)$. Superscript "+" and "−" represent $\partial E_f/\partial t > 0$ and $\partial E_f/\partial t < 0$, respectively. $P_{\mathrm{rev},j}(v_j)$ represents the reversible component in Eq. (7). In this model, n, w_j, v_j, and r_j are parameters for fitting to the shape of a given major hysteresis loop by superposition of a number of Preisach distribution functions (see Appendix).

Suppose $E_f = 0$ and $P_f = 0$ initially. When E_f increases monotonically, the derivative of polarization with respect to E_f is (see Appendix)

$$\frac{\partial P^+_{f,0}(E_f)}{\partial E_f} = \sum_{j=1}^{n} w_j \frac{\partial P^+_{j,0}(r_j, v_j)}{\partial E_f}, \tag{11}$$

where

$$\begin{aligned}\frac{\partial P^+_{j,0}(r_j, v_j)}{\partial E_f} = {} & \frac{P_s(1-r_j)\kappa}{4v_j} \operatorname{sech}^2\left(\frac{E_f - h}{v_j}\right) \\ & \times \left[1 - \tanh\left(\frac{E_f - h}{v_j}\right)\right]\left[\operatorname{sech}^2\left(\frac{E_f - h}{v_j}\right)\right. \\ & - \operatorname{sech}^2\left(\frac{E_f + h}{v_j}\right) + 2\tanh\left(\frac{E_f - h}{v_j}\right) \\ & \left. + 2\tanh\left(\frac{E_f + h}{v_j}\right)\right] + r_j \frac{\partial P_{\mathrm{rev},j}(v_j)}{\partial E_f}. \end{aligned} \tag{12}$$

If E_f increases from E_0 to E_1 such that $E_0 \leqslant E_f < E_1$, where E_0 and E_1 are two successive extrema of the field history, then the derivative of polarization is (see Appendix)

$$\frac{\partial P^+_f(E_f, E_0)}{\partial E_f} = \sum_{j=1}^{n} w_j \frac{\partial P^+_j(r_j, v_j)}{\partial E_f}, \tag{13}$$

where

$$\begin{aligned}\frac{\partial P^+_j(r_j, v_j)}{\partial E_f} = {} & \frac{P_s(1-r_j)\kappa}{4v_j} \operatorname{sech}^2\left(\frac{E_f - h}{v_j}\right) \\ & \times \left[1 - \tanh\left(\frac{E_f - h}{v_j}\right)\right]\left[\operatorname{sech}^2\left(\frac{E_0 + h}{v_j}\right)\right. \\ & - \operatorname{sech}^2\left(\frac{E_f + h}{v_j}\right) - 2\tanh\left(\frac{E_0 + h}{v_j}\right) \\ & \left. + 2\tanh\left(\frac{E_f + h}{v_j}\right)\right] + r_j \frac{\partial P_{\mathrm{rev},j}(v_j)}{\partial E_f}. \end{aligned} \tag{14}$$

For decreasing E_f (i.e., $\partial E_f/\partial t < 0$), explicit expressions for $\partial P^-_{j,0}(E_f)/\partial E_f$ and $\partial P^-_j(E_f, E_0)/\partial E_f$ may also be written by using the following relations: $\partial P^-_{j,0}(E_f)/\partial E_f = \partial P^+_{j,0}(-E_f)/\partial E_f$ and $\partial P^-_j(E_f, E_0)/\partial E_f = \partial P^+_j(-E_f, -E_0)/\partial E_f$.

III. METHODOLOGY FOR MEASUREMENT OF DIELECTRICITY

To investigate the bias-field-dependent dielectricity of a ferroelectric sample, the external field E_a in Eq. (4) is set as follows: a small measuring ac electric field E_a^{ac} with high frequency is superimposed on a dc bias field E_a^{dc}. After a measurement is made, the bias field is adjusted for another measurement. In this work, E_a^{ac} is taken as a sinusoidal wave and a typical schedule of E_a is shown in Fig. 1(a). In the figure, we assume 20 measurements for E_a ramping up and another 20 measurements for ramping down (40 measurements in total). Figure 1(b) shows a typical dc bias field E_a^{dc} followed by the measuring sinusoidal field $E_a^{\mathrm{ac}} \sim \sin \omega t$. For the sake of illustration, only four ac cycles are shown for each measurement. In our simulations, more ac cycles for E_a^{ac} are adopted so that a steady-state value for each measurement is obtained.

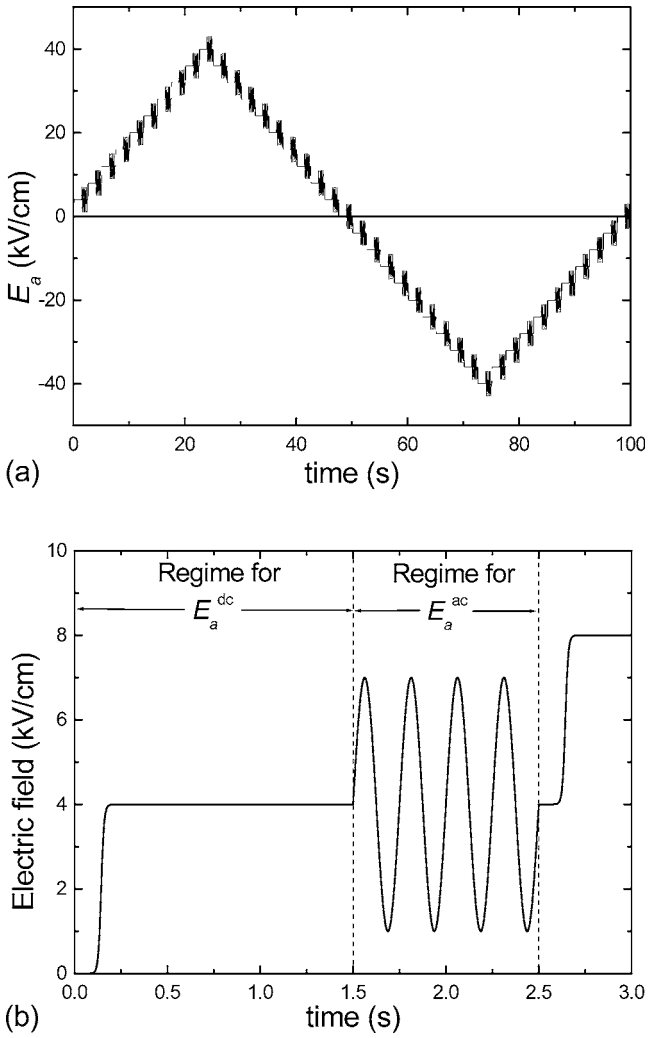

FIG. 1. (a) The time variation of E_a for implementing the methodology in Sec. III. The figure assumes 20 measurements per cycle. (b) A typical applied field schedule to measure permittivity. E_a increases by a step followed by a sequence of ac cycles for each permittivity measurement.

In this work, we have taken $n = 5$ in Eq. (6) to compose a saturated loop (major loop) for the barium zirconate titanate (BZT) and lead zirconate titanate (PZT), and the results are shown in Fig. 2. Our adopted $P_{f,\mathrm{sat}}$-E_f loop for model calculation has $P_s = 3.426\ \mu\mathrm{C/cm^2}$, $E_c = 7.5$ kV/cm and $P_s = 23.9\ \mu\mathrm{C/cm^2}$, $E_c = 33$ kV/cm for BZT and PZT, respectively. Other parameters including w_j, r_j, and v_j are listed in Tables I and II. Taking the saturated loop ($P_{f,\mathrm{sat}}$-E_f) of BZT in Fig. 2(a) as an example to solve Eq. (4), together with the parameters listed in Table III, we obtain a "fatter" hysteresis

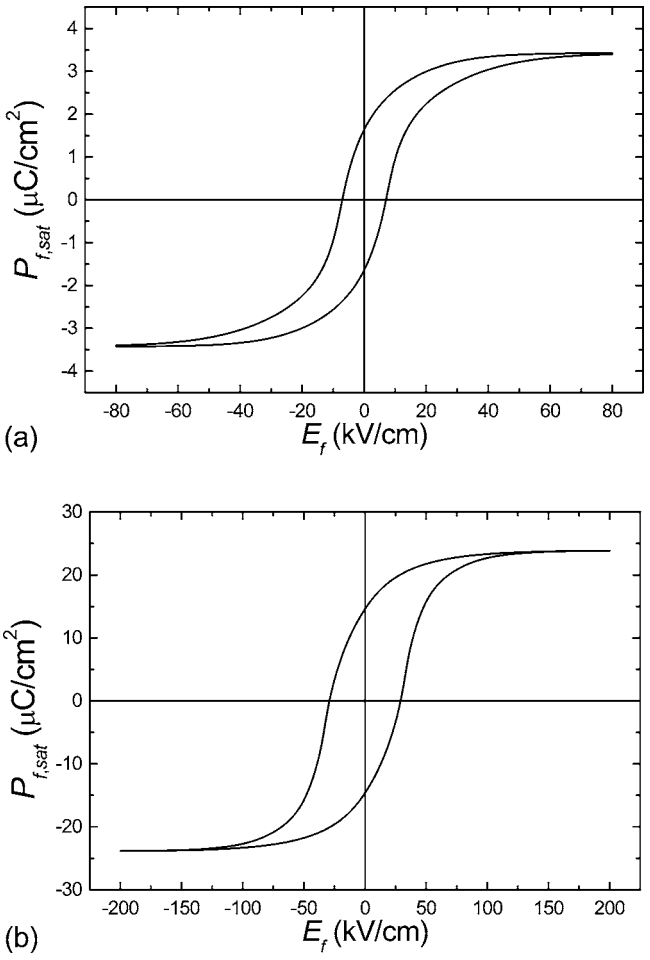

FIG. 2. Adopted *P-E* hysteresis loop of (a) BZT and (b) PZT predicted by Eq. (6) for model calculation.

loop shape comprising a set of "small" D^{ac}-E_a^{ac} hysteresis loops, such as shown in Fig. 3 (see Sec. IV for description). Each D^{ac}-E_a^{ac} loop is used to obtain a permittivity value which eventually leads to a profile of dielectricity with bias-field dependence. Using the Fourier transform technique, the electric field $E_a^{ac}(t)$ and the electric displacement $D^{ac}(t)$ of the film can be expressed as

$$E_a^{ac}(t) = E_0^{ac} + \sum_{n=1}^{\infty} [E_n^{ac\prime} \cos(n\omega t) + E_n^{ac\prime\prime} \sin(n\omega t)], \quad (15)$$

$$D^{ac}(t) = D_0^{ac\prime} + \sum_{n=1}^{\infty} [D_n^{ac\prime} \cos(n\omega t) + D_n^{ac\prime\prime} \sin(n\omega t)], \quad (16)$$

where E_0^{ac} and D_0^{ac} are constants, $E_n^{ac\prime}$ and $E_n^{ac\prime\prime}$ are the *n*th-order Fourier coefficients of $E_a^{ac}(t)$, and $D_n^{ac\prime}$ and $D_n^{ac\prime\prime}$ are

TABLE I. Preisach parameters (w_j, r_j, and v_j) for the hysteresis loop of BZT shown in Fig. 2(a).

j	w_j	r_j	v_j(kV/cm)
1	0.1	0	3
2	0.2	0.88×10^{-2}	7
3	0.1	0.438	13
4	0.1	0.496	18
5	0.5	0	50

TABLE II. Preisach parameters (w_j, r_j, and v_j) for the hysteresis loop of PZT shown in Fig. 2(b).

j	w_j	r_j	v_j(kV/cm)
1	0.1	0.02	5
2	0.45	0.084	20
3	0.15	0.17	50
4	0.15	0.38	60
5	0.15	0.84	80

the *n*th-order Fourier coefficients of $D^{ac}(t)$. The "measured" linear permittivity is calculated by

$$\varepsilon = D_1^{ac\prime\prime}/E_1^{ac\prime\prime}. \quad (17)$$

From Eq. (17), the dielectric constant ($\varepsilon_r = \varepsilon/\varepsilon_0$ where ε_0 is the permittivity of vacuum) for each D^{ac}-E_a^{ac} hysteresis loop can be calculated. Thus, the variation of dielectric constant ε_r of the ferroelectric with bias electric field E_{bi} is also obtained. The corresponding dielectric tunability Q of the material is defined as

$$Q = \left| \frac{\max\{\varepsilon_r\} - \min\{\varepsilon_r\}}{\max\{\varepsilon_r\}} \right|. \quad (18)$$

IV. RESULTS AND DISCUSSION

A. Modeling parameters and the hysteresis loops of ferroelectric films

Tohma *et al.* have measured the *D-E* loop of a BZT thin film at 100 Hz and the bias-field-dependent permittivity.[2] The amplitude of E_a^{ac} is 1.5 kV/cm and the permittivity measurement is set at 100 kHz. We have composed a saturated loop for the bulk region of BZT [Fig. 2(a)] with the parameters adopted in Eq. (6) shown in Table I. These parameters will also be adopted for the calculations of unsaturated loops by using Eqs. (11) and (13). Other properties of BZT adopted for the calculations are shown in Table III. As dead layers are normally thin with a reduced dielectricity than in the rest of the film,[12,23] we have therefore adopted $\nu=0.05$, $\varepsilon_f=310\varepsilon_0$, and $\varepsilon_d=260\varepsilon_0$. Since ε in our model denotes the slope of a *D-E* loop at $P=P_s$ [see Eq. (1)], the values for ε_f and ε_d are chosen in a way that the calculated ε_r of the BZT film agree well with the experimental values at the highest bias field.[2] Using the saturated loop in Fig. 2(a) and assuming $\rho_i = 0.7\ \mu C/cm^2$ (i.e., uniform ρ within the dead layer), $m=20$, and $\sigma_f=\sigma_d=5\times10^{-13}\ \Omega^{-1}\ cm^{-1}$, simulated results of the *D*-E_a hysteresis loops for the BZT thin film are shown in Figs. 3 and 4(a). The hysteresis loop in Fig. 4(a) is traced by a sinusoidal wave of 100 Hz,[2] while those in Fig. 3 are traced by a schedule for E_a similar to that in Fig. 1(a), but 56 measurements per cycle are adopted rather than 40 in Fig. 1(a). The result upon Fourier transforming the minor loops in Fig. 3 becomes a ε_r-E_{bi} loop. Comparison of our simulated results with the experimental data for *D-E* and ε_r-E_{bi} loops are shown in Figs. 4(a) and 5, respectively.

Vieitez *et al.* have also measured the *D-E* and ε-*E* loops of a PZT thin film.[1] The hysteresis loop is traced at 65 Hz and the permittivity measurement is set at 1 kHz with 1.5 s

TABLE III. Material parameters of BZT and PZT adopted in this work.

	ν	$\varepsilon_f/\varepsilon_0$	$\varepsilon_d/\varepsilon_0$	P_s (μC/cm^2)	E_c (kV/cm)	$\sigma=\sigma_f=\sigma_d$ (Ω^{-1} cm^{-1})	ρ (μC/cm^2)
BZT	0.05	310	260	3.426	7.5	5×10^{-13}	0.7
PZT	0.05	600	550	23.9	33	50×10^{-13}	0

of sampling delay. Our composed saturated loop for the bulk region of PZT is shown in Fig. 2(b) and the parameters adopted in Eqs. (4)–(6), (11), and (13) are listed in Tables II and III. Since both the D-E and ε-E loops measured by Vieitez *et al.* are almost symmetrical, we have set $\rho_i=0$ and $m=1$ (i.e., no initial trapped charge). Using the saturated loop in Fig. 2(b) and taking $\nu=0.05$, $\varepsilon_f=600\varepsilon_0$, $\varepsilon_d=550\varepsilon_0$, $\sigma_f=\sigma_d=50\times10^{-13}$ Ω^{-1} cm^{-1}, and $E_a^{ac}=6.8$ kV/cm (i.e., 1/25 of the largest bias field used by Vieitez *et al.*), simulated results for D-E_a and ε_r-E_{bi} loops are shown in Figs. 4(b) and 6, respectively. Comparisons with experimental data have also been made in these figures. Similar to the treatment of the BZT system, the values for ε_f and ε_d are also chosen in a way that the calculated ε_r agree well with the experimental values at the highest bias field.[1]

Figure 4 demonstrates that our proposed model is able to fit reasonable well to the D-E curves of BZT and PZT thin films. In Fig. 4(a), a clear horizontal shift of the hysteresis loop is shown. This phenomenon has been discussed in the literature and a possible origin is the trapped charge in the dead layer of the film. Although our modeled shift magnitude is larger than the experimental, the loop shape is very close to that measured. The simulated loop shown in Fig. 4 is the second cycle after the application of the external ac field.

B. Comparison with experimental ε_r-E_{bi} loops

Figure 5(a) shows the comparison between our modeled results and the experimental data of bias-field-dependent permittivity for BZT. Using the same constituent properties as for modeling the D-E loop in Fig. 4(a), the simulated permittivity of the BZT thin film is obtained by using the methodology given in Sec. III. Each bias-field-dependent permittivity is based on the corresponding minor loop which should be very close to the steady state. We see in Fig. 5(a) that almost all features of the experimental curve can be reproduced. Note that the horizontal shift is more significant when E_a is ramped down (decreasing field) [versus when E_a is ramped up]. This feature is also roughly reproduced by our simulation, even though our modeled ε_r-E_{bi} loop has a slightly smaller horizontal shift than experiment for the region of positive bias fields. The dielectric tunability which is about 53% [calculated by Eq. (18)] has been faithfully reproduced by our model. In Fig. 5(b), an alternative definition to calculate the ε_r of BZT thin film is adopted and results are compared with the experimental data. Here ε_r is obtained from the slope of the D-E loop traced by an external sinusoidal field (i.e., the derivative of D with respect to the electric field E, conventionally adopted by many authors). It is seen that this ε_r curve is very far away from that of the

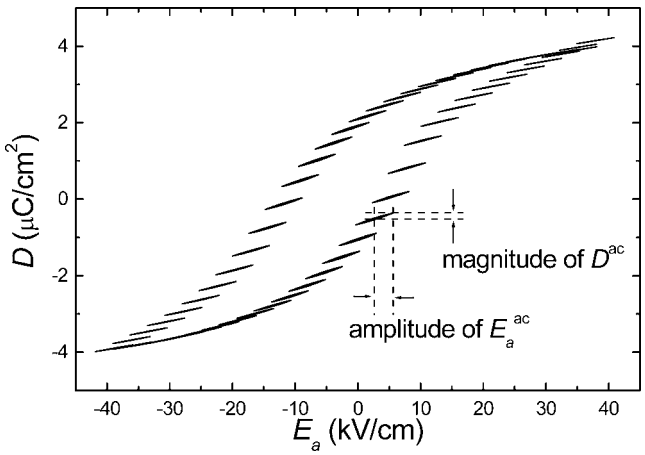

FIG. 3. Simulated D-E_a hysteresis loops with E_a following a schedule similar to that shown in Fig. 1.

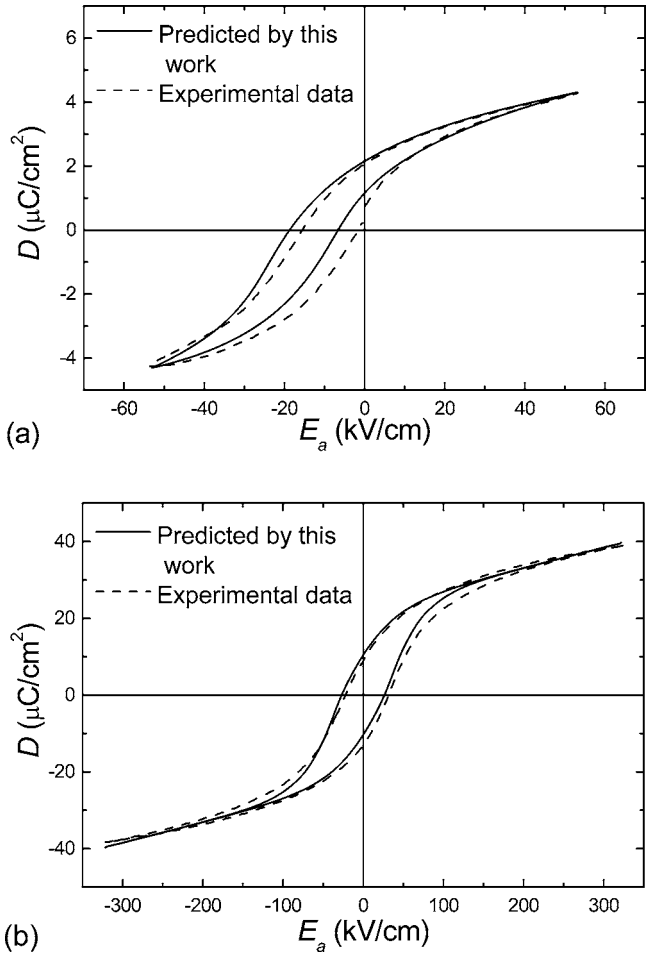

FIG. 4. Comparison of theoretical prediction for the D-E hysteresis loop of (a) BZT thin film with the experimental data of Tohma *et al.* (see Ref. 2) and (b) PZT thin film with the experimental data of Vieitez *et al.* (see Ref. 1).

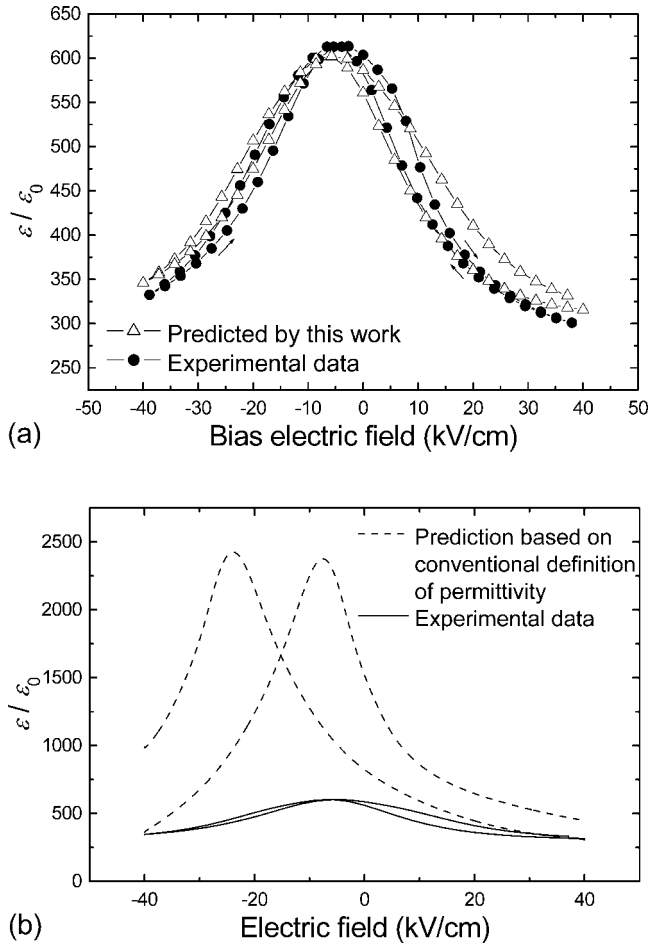

FIG. 5. Comparison of theoretical predictions for the ε_r-$E_{\rm bi}$ loop of BZT thin film with the experimental data of Tohma *et al.* (see Ref. 2). (a) The methodology in Sec. III is adopted; (b) ε_r is calculated from the derivative of D with respect to the electric field and E_a is a sinusoidal field.

experimental curve. We can conclude that the experimental permittivity is not equal to the widely accepted "theoretical permittivity."

Concerning the comparison between our modeled ε_r-$E_{\rm bi}$ loop and the experimental data of Vieitez *et al.* for PZT, fairly good agreement is also obtained (Fig. 6). The

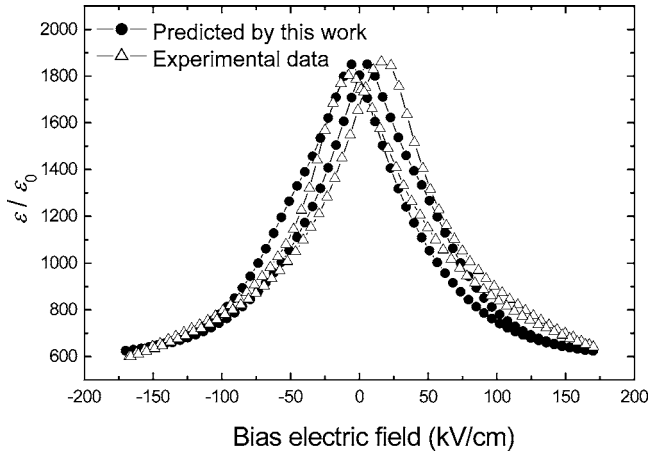

FIG. 6. Comparison of theoretical predictions for the ε_r-$E_{\rm bi}$ loop of PZT thin film with the experimental data of Vieitez *et al.* (see Ref. 1).

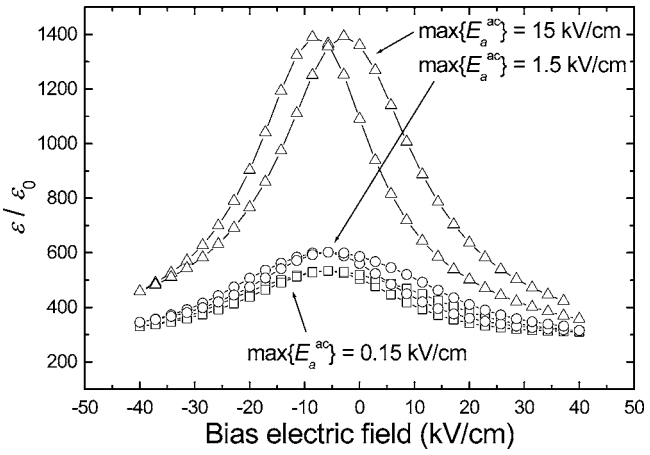

FIG. 7. Variation of the simulated ε_r-$E_{\rm bi}$ loop with the amplitude of $E_a^{\rm ac}$.

experiment constitutes 60 measurements for E_a ramping up and another 60 measurements for ramping down (120 measurements in total). The experiment showed a maximum tunability of 68% under a bias field of 170 kV/cm. This tunability was equally high as compared to 70% reported for the PZT thin film [also $Pb(Zr_{0.52}Ti_{0.48})O_3$] under a bias of about 300 kV/cm by Maleto *et al.*[24] If a much higher bias field is adopted by Vieitez *et al.*, larger tunability of ε_r than that shown in Fig. 6 may be possible.

C. Effects of ac measurement field and charge density on the horizontally shifted ε_r-$E_{\rm bi}$ loops of BZT

Apart from the above, we have also tried different parameters in the calculations on the bias-field-dependent permittivity. Hereafter, we concentrate on the system of BZT. First, we use different amplitudes of $E_a^{\rm ac}$ [denoted by $\max\{E_a^{\rm ac}\}$] to recalculate the ε_r-$E_{\rm bi}$ loop. Figure 7 shows that a larger $E_a^{\rm ac}$ amplitude can increase the permittivities at all bias fields under investigation. The dielectric tunability also increases as the amplitude of $E_a^{\rm ac}$ increases. This is consistent with the finding of Tohma *et al.*[2] In the figure, the largest $\max\{E_a^{\rm ac}\}$(=15 kV/cm) is twice the coercive field of BZT, which may be much larger than is used in most practical measurements. However, this field strength is still much smaller than the required value to trace $D^{\rm ac}$-$E_a^{\rm ac}$ loops similar with the saturated loop [see Fig. 2(a)]. Thus the calculated maximum ε_r is still smaller than the "conventional" values shown in Fig. 5(b). In addition, the decrement of permittivities for decreasing $\max\{E_a^{\rm ac}\}$ shown in Fig. 7 will actually continue until $\max\{E_a^{\rm ac}\} \approx 0.05$ kV/cm. When $\max\{E_a^{\rm ac}\} < 0.05$ kV/cm, steady state is reached and no further notable decrement is observed. One more point to note from Fig. 7 [also Fig. 5(a)] is that all permittivities shown are larger than the values adopted for ε_f and ε_d. This feature will not emerge if we do not consider the role of the ferroelectric hysteresis loop.

The profile of the ε_r-$E_{\rm bi}$ loop is also affected by the number of measurements. In Figs. 5(a) and 7, we used 56 measurements (28 measurements for ramp up and another 28 measurements for ramp down) versus 54 measurements performed by Tohma *et al.* Now we use 28 and 112 measurements to recalculate the ε_r-$E_{\rm bi}$ loop. Figure 8 shows that this

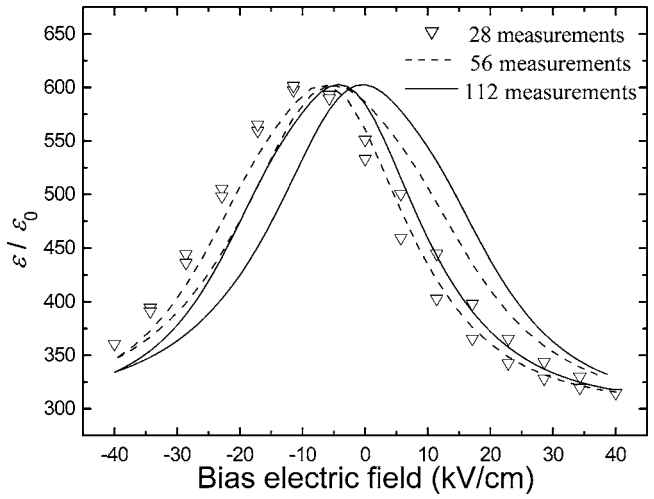

FIG. 8. Variation of the simulated ε_r-E_{bi} loop with the number of measurements for a field cycle (ramp up and ramp down).

variation does not have much effect on the extrema values of dielectric constant and hence tunability. However, an increased number of measurements tends to reduce the horizontal shift of the ε_r-E_{bi} loop. This is essentially the effect of the finite conductivity of the materials, which gives rise to charge flow and influences the charge density. A greater number of measurements allows charges more redistribution time, but using a smaller σ value would slow the charge movement. Hence, the number of measurements may have negligible effect for low-conductivity films unless the measurement time is sufficiently long.

In Fig. 9, different values of charge density ρ_i have been adopted to examine the horizontal shift phenomenon in the ε_r-E_{bi} loop. In the figure, all the modeled results use the same constituent parameters as in Fig. 5(a) with uniform profile of ρ_i. Only the increasing branches of these curves are shown in the figure for the sake of clarity. When the passive layer has $\rho_i=0$, the ε_r-E_{bi} loop centers at the origin. However, the decreasing branch (not shown) of the ε_r-E_{bi} loop remains slightly left shifted relative to the increasing branch. This phenomenon is normal and can be noted from previous

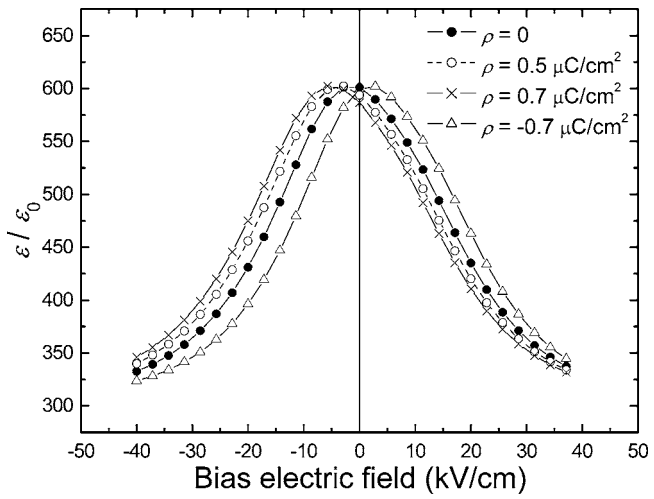

FIG. 9. Variation of the simulated ε_r-E_{bi} loop with the magnitude of a uniform charge density in the passive layer.

experimental results.[2–4] For $\rho_i=0.5\ \mu\mathrm{C/cm^2}$, a notable horizontal shift is observed. Suppose ρ_i is increased further to $0.7\ \mu\mathrm{C/cm^2}$, a more pronounced horizontal shift is observed [the same set of parameters as adopted for Fig. 5(a)]. We also found that near maximum horizontal shift is already achieved for ρ_i slightly larger than $0.7\ \mu\mathrm{C/cm^2}$. When the sign of ρ_i is negative, the ε_r-E_{bi} loop shifts to the opposite direction with slightly smaller shift magnitude. We will obtain an unchanged shift magnitude of ε_r-E_{bi} loop for $\rho_i=-0.7\ \mu\mathrm{C/cm^2}$ (as for $\rho_i=0.7\ \mu\mathrm{C/cm^2}$) if we first trace the negative bias fields before the positive bias fields. The above analyses have been confined to the ε_r-E_{bi} loops. Actually, the general feature of horizontal shift induced by a higher or lower ρ is identical in the D-E_a loop (i.e., a larger magnitude of ρ gives more shift and its sign determines the shift direction). In view of the shift phenomenon demonstrated above for both ε_r-E_{bi} and D-E_a loops, the origin of horizontal shift observed in the experimental data of Vieitez *et al.* and Tohma *et al.* may very well be originated from the charged dead layer in the films.

In the above analysis, we have introduced a passive nonferroelectric layer at the film-electrode interface to model the inhomogeneity of polarization and permittivity across the interface. We have also assumed that this layer possesses uniform permittivity and charge density. This approach had already been able to demonstrate that a charged dead layer is able to lead to horizontal offsets observed in experiments. Actually, structural or other variations adjacent to the interface between the bulk and dead layers are expected to be gradual. If $D_{d,i}=\varepsilon_{d,i}E_d+P_{d,i}$ is substituted for the second equation in Eqs. (1), the model can also be used to study D-E_a and ε_r-E_{bi} loops with nonuniform profile of $\varepsilon_{d,i}$, $P_{d,i}$, and ρ_i. However, so far only very few experimental investigations have been performed to study the variations of such parameters adjacent to the film-electrode interface.

V. CONCLUSIONS

The bias-field-dependent permittivity of BZT and PZT thin films has been studied by assuming a dead layer region is formed at the film-electrode interface, which possesses reduced dielectricity and ferroelectricity. The presence of this region is conveniently tackled by a multilayer model. The simulated unsaturated D-E loops are Fourier transformed to obtain the ε_r-E_{bi} loop. Comparison with experimental data shows good agreement. In contrast, theoretical calculations of ε_r based on the derivative of D with respect to E for the major hysteresis loop do not fit well with the measured values. This confirms that consideration of minor hysteresis loops is essential. Our simulated ε_r-E_{bi} loop for the BZT thin film shows an asymmetric behavior of high dielectric tunability which is found to be significantly affected by the ac component in the applied field schedule. When initially trapped charge is given to the dead layer region, the ε_r-E_{bi} loop reveals a horizontal shift, analogous to the shift phenomenon for the D-E loops frequently revealed in thin films.

ACKNOWLEDGMENT

This work was partially supported by the Center for Smart Materials of The Hong Kong Polytechnic University.

APPENDIX

In the Preisach model,[9,11] the polarization of the ascending and descending major curves of a hysteresis loop can be written as

$$P_{\mathrm{sat}}^{+}(E) = -P_s + 2P_s \int_{-\infty}^{E}\int_{-\infty}^{U} \wp(U,V)\,dV\,dU, \tag{A1}$$

$$P_{\mathrm{sat}}^{-}(E) = P_s - 2P_s \int_{E}^{\infty}\int_{V}^{\infty} \wp(U,V)\,dU\,dV = -P_{\mathrm{sat}}^{+}(-E), \tag{A2}$$

where $\wp(U,V)$ is the normalized Preisach distribution function which may be divided into two components: irreversible and reversible components, i.e.,

$$\wp(U,V) = (1-r)\wp_{\mathrm{irr}}(U,V) + r\wp_{\mathrm{rev}}(U,V). \tag{A3}$$

r is the weight of the reversible component in the Preisach function and P_s represents saturation polarization. Now consider a virgin material (no residual fields initially) on which a field E is applied. The derivative of polarization respect to E is

$$\partial P_0^{+}(E)/\partial E = 2P_s \int_{-E}^{E} \wp(E,V)\,dV, \tag{A4}$$

$$\partial P_0^{-}(E)/\partial E = 2P_s \int_{E}^{-E} \wp(U,E)\,dU = \partial P_0^{+}(-E)/\partial E, \tag{A5}$$

when the applied field E is increasing and decreasing, respectively. Assume that E_0 and E_1 are two successive extrema of the field history and $E_0 < E_1$. If now the applied field E increases from E_0 to E such that $E_0 \leqslant E < E_1$, the derivative of polarization respect to E is

$$\partial P^{+}(E,E_0)/\partial E = 2P_s \int_{E_0}^{E} \wp(E,V)\,dV. \tag{A6}$$

For $E_0 > E_1$ and the applied field E decreases from E_0 to E such that $E_0 \geqslant E > E_1$, the derivative of polarization respect to E is

$$\partial P^{-}(E,E_0)/\partial E = 2P_s \int_{E}^{E_0} \wp(U,E)\,dU = \partial P^{+}(-E,-E_0)/\partial E. \tag{A7}$$

Using Eqs. (A1)–(A7), the polarization of a ferroelectric material after going through an arbitrary field history can be calculated.

In this work, the irreversible Preisach function $\wp_{\mathrm{irr}}(U,V)$ is assumed to be a product of distributions of U and V:

$$\wp_{\mathrm{irr}}(U,V) = \frac{1}{2\upsilon}\,\mathrm{sech}^2\!\left(\frac{U-h}{\upsilon}\right)\left[1-\tanh\!\left(\frac{U-h}{\upsilon}\right)\right] \times \frac{1}{2\upsilon}\,\mathrm{sech}^2\!\left(\frac{V+h}{\upsilon}\right)\left[1-\tanh\!\left(\frac{V+h}{\upsilon}\right)\right], \tag{A8}$$

where

$$h = \upsilon \ln \times \sqrt{1 - 2\cosh^2(E_c/\upsilon) + 10\cosh(E_c/\upsilon)\sqrt{\cosh^2(E_c/\upsilon)-1}}$$

and E_c denotes coercive field. The factor υ is an adjustable parameter to fit the shape of the experimental major curve. It essentially describes the dispersion of the distributions of U and V. Note that the expression for polarization depends on the history of the field applied onto the material. The advantage in choosing this function is that it can provide explicit forms for arbitrary reversal polarization curves, the virgin curve (from $P=0$), and major loop of a ferroelectric. The reversible Preisach function $\wp_{\mathrm{rev}}(U,V)$ is taken as

$$\wp_{\mathrm{rev}}(U,V) = \delta(U-V)\frac{\mathrm{sech}^2(U/\upsilon)}{\upsilon}, \tag{A9}$$

where δ is the Dirac delta function. The closed form expression obtained by putting Eqs. (A3), (A8), and (A9) into Eq. (A1) is

$$\begin{aligned} P_{\mathrm{sat}}^{+}(E) = \frac{P_s(1-r)\kappa}{8}\Bigg\{ & 2\coth\!\left(\frac{2h}{\upsilon}\right)\left[4\,\mathrm{csch}^2\!\left(\frac{2h}{\upsilon}\right)\ln\!\left(\frac{\cosh[(E-h)/\upsilon]}{\cosh[(E+h)/\upsilon]}\right)+\mathrm{sech}^2\!\left(\frac{E-h}{\upsilon}\right)\right] \\ & + 4\coth^3\!\left(\frac{2h}{\upsilon}\right)\tanh\!\left(\frac{E-h}{\upsilon}\right)+\mathrm{csch}^2\!\left(\frac{2h}{\upsilon}\right)\left[2\left(1+2\cosh\!\left(\frac{4h}{\upsilon_j}\right)\right)\mathrm{csch}^2\!\left(\frac{2h}{\upsilon}\right)\right. \\ & \times \ln\!\left(\frac{\cosh[(E-h)/\upsilon]}{\cosh[(E+h)/\upsilon]}\right)+\cosh\!\left(\frac{4h}{\upsilon}\right)\mathrm{sech}^2\!\left(\frac{E-h}{\upsilon}\right)+2\left(\mathrm{sech}\!\left(\frac{2h}{\upsilon}\right)+\mathrm{csch}\!\left(\frac{2h}{\upsilon}\right)\right) \\ & \left.\times\,\mathrm{sech}\!\left(\frac{E+h}{\upsilon}\right)\sinh\!\left(\frac{E-h}{\upsilon}\right)+2\left(2+\cosh\!\left(\frac{4h}{\upsilon}\right)\right)\tanh\!\left(\frac{E-h}{\upsilon}\right)\right]\Bigg\}+rP_{\mathrm{rev}}(E), \end{aligned} \tag{A10}$$

where

$$\kappa = \frac{-8\exp(-4h/\upsilon)\upsilon\sinh^4(2h/\upsilon)}{8h-2\upsilon+2(2h+\upsilon)\cosh(4h/\upsilon)-(4h+3\upsilon)\sinh(4h/\upsilon)}, \tag{A11}$$

$$P_{\mathrm{rev}}(E) = P_s\tanh(E/\upsilon), \tag{A12}$$

and the closed form expressions for Eqs. (A4) and (A6) after substituting Eqs. (A3), (A8), and (A9) are

$$\begin{aligned}\frac{\partial P_0^+(E)}{\partial E} = {} & \frac{P_s(1-r)\kappa}{4\upsilon}\mathrm{sech}^2\left(\frac{E-h}{\upsilon}\right)\left[1-\tanh\left(\frac{E-h}{\upsilon}\right)\right] \\ & \times\left[\mathrm{sech}^2\left(\frac{E-h}{\upsilon}\right)-\mathrm{sech}^2\left(\frac{E+h}{\upsilon}\right)\right. \\ & \left.+2\tanh\left(\frac{E-h}{\upsilon}\right)+2\tanh\left(\frac{E+h}{\upsilon}\right)\right] \\ & +r\frac{\partial P_{\mathrm{rev}}(E)}{\partial E},\end{aligned} \tag{A13}$$

$$\begin{aligned}\frac{\partial P^+(E,E_0)}{\partial E} = {} & \frac{P_s(1-r)\kappa}{4\upsilon}\mathrm{sech}^2\left(\frac{E-h}{\upsilon}\right) \\ & \times\left[1-\tanh\left(\frac{E-h}{\upsilon}\right)\right]\left[\mathrm{sech}^2\left(\frac{E_0+h}{\upsilon}\right)\right. \\ & -\mathrm{sech}^2\left(\frac{E+h}{\upsilon}\right)-2\tanh\left(\frac{E_0+h}{\upsilon}\right) \\ & \left.+2\tanh\left(\frac{E+h}{\upsilon}\right)\right]+r\frac{\partial P_{\mathrm{rev}}(E)}{\partial E}.\end{aligned} \tag{A14}$$

The closed form expressions for Eqs. (A2), (A5), and (A7) can also be derived in a similar way.

In general, the presently adopted form of Preisach functions [Eqs. (A8) and (A9)] may only describe limited kinds of hysteresis loop shapes. To extend the usage of this model for a broader variety of loop shapes, the polarization major curve may be written as a linear combination of the standard shape described by Eq. (A10) with each one having its own set of r and υ (distinguished by subscript j). Hence,

$$P_{f,\mathrm{sat}}^+(E_f) = \sum_{j=1}^{n} w_j P_{\mathrm{sat},j}^+(r_j,\upsilon_j), \tag{A15}$$

and for the derivative of unsaturated polarizations:

$$\frac{\partial P_{f,0}^+(E_f)}{\partial E_f} = \sum_{j=1}^{n} w_j\frac{\partial P_{j,0}^+(r_j,\upsilon_j)}{\partial E_f}, \tag{A16}$$

$$\frac{\partial P_f^+(E_f,E_0)}{\partial E_f} = \sum_{j=1}^{n} w_j\frac{\partial P_j^+(r_j,\upsilon_j)}{\partial E_f}, \tag{A17}$$

where $\partial P_{j,0}^+(r_j,\upsilon_j)/\partial E_f$ and $\partial P_j^+(r_j,\upsilon_j)/\partial E_f$ are calculated by Eqs. (A13) and (A14), respectively. The quantities appearing on the left-hand side of Eqs. (A15)–(A17) are adopted in Eq. (4). The values of w_j, r_j, and υ_j may be obtained by fitting mathematically to experimental loops using Eq. (A15) if measurement of the major curve is available. Otherwise, they may also be judiciously chosen for the shape of some standard major loops.

[1] M. O. Vieitez, S. I. Khartsev, and A. M. Grishin, *Ferroelectric Thin Films XI Symposium*, Boston, Dec. 2–5, 2002 (Materials Research Society, 2003), Vol. 748, p. 325.
[2] T. Tohma, H. Masumoto, and T. Goto, Jpn. J. Appl. Phys., Part 1 **42**, 6969 (2003).
[3] A. Jiang, M. Dawber, J. F. Scott, C. Wang, P. Migliorato, and M. Gregg, Jpn. J. Appl. Phys., Part 1 **42**, 6973 (2003).
[4] R. G. Mendes, I. A. Santos, E. B. Araújo, and J. A. Eiras, Ferroelectrics **271**, 1837 (2002).
[5] S. L. Miller, J. R. Schwank, R. D. Nasby, and M. S. Rodgers, J. Appl. Phys. **70**, 2849 (1991).
[6] Y. T. Or, C. K. Wong, B. Ploss, and F. G. Shin, J. Appl. Phys. **93**, 4112 (2003).
[7] Y. T. Or, C. K. Wong, B. Ploss, and F. G. Shin, J. Appl. Phys. **94**, 3319 (2003).
[8] C. K. Wong and F. G. Shin, Appl. Phys. Lett. **86**, 042901 (2005).
[9] E. D. Torre, *Magnetic Hysteresis* (IEEE, New York, 1999), Chap. 5.
[10] B. Jiang, J. C. Lee, P. Zurcher, and R. E. Jones, Jr., Integr. Ferroelectr. **16**, 805 (1997).
[11] F. Preisach, Z. Phys. **94**, 277 (1935).
[12] G. Le Rhun, R. Bouregba, and G. Poullain, J. Appl. Phys. **96**, 5712 (2004).
[13] J. Lee, R. Ramesh, V. G. Keramidas, W. L. Warren, G. E. Pike, and J. T. Evans, Jr., Appl. Phys. Lett. **66**, 1337 (1995).
[14] V. C. Lo, J. Appl. Phys. **92**, 6778 (2002).
[15] W. Wu, K. H. Wong, and C. L. Choy, Appl. Phys. Lett. **85**, 5013 (2004).
[16] W. Wu, Y. Wang, G. K. H. Pang, K. H. Wong, and C. L. Choy, Appl. Phys. Lett. **85**, 1583 (2004).
[17] M. Grossmann, O. Lohse, D. Bolten, U. Boettger, T. Schneller, and R. Waser, J. Appl. Phys. **92**, 2680 (2002).
[18] W. L. Warren, G. E. Pike, B. A. Tuttle, and D. Dimos, Appl. Phys. Lett. **70**, 2010 (1997).
[19] E. G. Lee, D. J. Wouters, G. Willems, and H. E. Maes, Appl. Phys. Lett. **69**, 1223 (1996).
[20] B. H. Park, T. W. Noh, J. Lee, C. Y. Kim, and W. Jo, Appl. Phys. Lett. **70**, 1101 (1997).
[21] S. Okamura, S. Miyata, Y. Mizutami, T. Nishida, and T. Shiosaki, Jpn. J. Appl. Phys., Part 1 **38**, 5364 (1999).
[22] C. Zhou and D. M. Newns, J. Appl. Phys. **82**, 3081 (1997).
[23] B. Chen *et al.*, Appl. Phys. Lett. **84**, 583 (2004).
[24] M. Maleto, E. Pevtsov, A. Sigov, and A. Svotina, Ferroelectrics **286**, 1023 (2003).